Acta Scientiarum
http://periodicos.uem.br/ojs/acta
ISSN on-line: 1807-8672
Doi: 10.4025/actascitechnol.v47i1.70816

Numerical analysis of the failure mode of reinforced concrete beams with glass fiber reinforced polymer bars

Victória Geovana Hollanda do Amaral*, Guilherme Francyan Teixeira Alves, Pedro Ignácio Lima Gadêlha Jardim and Diego Henrique de Almeida

Universidade Federal de Rondônia, Rodovia BR-364, s/n, km 9,5, 76801-059, Porto Velho, Rondônia, Brazil. *Author for correspondence. E-mail: victoriahollanda17@gmail.com

ABSTRACT. The durability of reinforced concrete structures can vary significantly depending on their specific application. One of the elements that has a negative impact on this durability is the corrosion of steel bars. In this context, several studies have been conducted with the aim of mitigating the incidence of this phenomenon, and such efforts include the replacement of conventional carbon steel bars with glass fiber reinforced polymer (GFRP) bars. The primary aim of this study is to analyze the impact of concrete properties on concrete beams reinforced with GFRP concerning bending stiffness and failure mode. To achieve this analysis, numerical simulations using the finite element method were carried out using the educational version of the Abaqus software. The most significant results of this investigation indicate that varying the α_E parameter, parameter depending on the type of aggregate used according to NBR 6118 (2014), for beams using steel as the reinforcement material is more advantageous in terms of increasing load capacity, when compared to varying the f_{ck}. However, the opposite behavior was observed in the beams using GFRP as the reinforcing material. In addition, it can be seen that the failure mode presented significant changes when the steel reinforcement is partially replaced by GFRP, due to the brittle nature inherent in the material.

Keywords: Finite element method; GFRP bars; numerical simulation; rupture mode.

Received on December 23, 2023.
Accepted on September 4, 2024.

Introduction

The use of different materials to replace or reinforce reinforced concrete structures has been the subject of study in the field of structural engineering. The durability of reinforced concrete structures varies according to their use, with 100 years being required for bridge structures, according to the National Department of Infrastructure and Transport (DNIT, 2010) and 50 years for residential buildings, according to the Brazilian Association of Technical Standards NBR 15575 (ABNT, 2013), entitled "Residential buildings - Performance".

Corrosion of steel bars is one of the factors that negatively influences the durability of reinforced concrete structures. It can occur through oxidation or electrochemical corrosion and is indicated as the main deleterious agent of steel used in reinforced concrete structures (Ribeiro et al., 2018). Thus, several studies have been carried out to reduce the occurrence of this phenomenon, with the replacement of traditional carbon steel bars with glass fiber-reinforced polymer (GFRP) bars being a promising option as it is an inert material with good durability indexes (Ineia et al., 2021).

In line with Chattopadhyay at al. (2018), GFRP bars have properties capable of guaranteeing strength and durability to concrete structures, and do not suffer from corrosion as they are an inert material. These characteristics allow this material to be used as a substitute for traditional steel bars, ensuring greater durability combined with adequate strength and ease of use.

Due to the difficulties encountered in the experimental study of GFRP and the fact that it is difficult to obtain, numerical studies have shown a good ability to predict and represent the behavior of this material (Alves et al., 2024). The aim of this work is to propose the FEM as a structural analysis tool for concrete beams reinforced with GFRP, as well as to evaluate the influence of GFRP as partial reinforcement on the failure mode of the beams.

Material and methods

A three-dimensional FE model was created to model the GFRP reinforced concrete (RC) beams. The experimental tests on concrete beam reinforced with steel and GFRP conducted by Dalfré et al. (2021) were adopted to verify the finite element model developed, with a concrete compressive strength (f_c) of 32.8 MPa, obtained experimentally. Dalfré et al. (2021) proposed two experimental models with longitudinal steel bars and an additional two models with partial substitution using GFRP bars. A parametric study was conducted analyzing 24 reinforced concrete beams, the lower reinforcement material, f_{ck} and the modulus of elasticity (E) were varied.

For the lower reinforcement material at first steel was used, and then GFRP were considered as a partial replacement of steel bars. The compressive strength adopted for RC beams was 30, 40 and 50MPa, aiming to analyze the compressive strength of concretes commonly used in standard buildings and small structures. Different modulus of elasticity utilized was obtained by Equation 1, defined by Brazilian Association of Technical Standards NBR 6118 (ABNT, 2023).

$$E = \alpha_i \, . \, E_i \tag{1}$$

$$E_i = \alpha_E \, . \, 5600 \, . \, \sqrt{f_{ck}} \tag{2}$$

$$\alpha_i = 0{,}8 + 0{,}2 \, . \, \frac{f_{ck}}{80} \leq 1{,}0 \tag{3}$$

In the Equation 2, the coefficient α_E varies according to the source rock of the coarse aggregate, which is 0,7 for sandstone, 0,9 for limestone, 1,0 for granite or gneiss and 1,2 for basalt or diabase. In this study, all the variations in the coefficient were considered. For each model, specific information has been assigned that constitutes its unique identity. In the nomenclature B stands for beams and the rest represents the variations considered in the nomenclature reflect different parameters and characteristics, such as the compressive strength of the concrete, the α_E coefficient, and the type of longitudinal reinforcement used. The nomenclature of each model is shown in Figure 1.

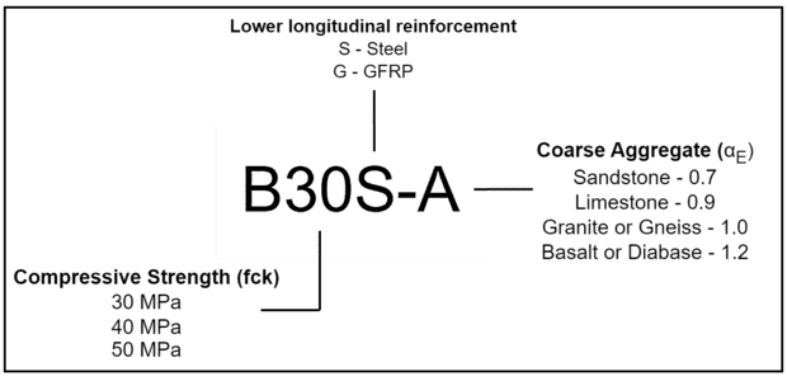

Figure 1. Nomenclature used for each model.

All the models were also identified with their respective modulus of elasticity, as shown in Table 1.

Table 1. Modulus of elasticity of each model.

Alphanumeric	E (MPa)	Alphanumeric	E (MPa)
B30S-A B30G-A	21470,7	B40S-C B40G-C	35417,5
B30S-B B30G-B	27605,2	B40S-D B40G-D	42501,0
B30S-C B30G-C	30672,5	B50S-A B50G-A	27718,6
B30S-D B30G-D	36806,9	B50S-B B50G-B	35638,2
B40S-A B40G-A	24792,3	B50S-C B50G-C	39597,9
B40S-B B40G-B	31875,8	B50S-D B50G-D	47517,6

Numerical study configuration

Beams were simulated using non-linear analyses. ABNT NBR 6118 (2023) was used to obtain the properties of concrete and steel bars, the behavior in the plastic state and in the rupture were predicted by the damage model called CDP (concrete damaged plasticity) presented by Guo (2014). The GFRP was considered linear (Figure 2b). The steel was defined with a bilinear stress-strain behavior (Figure 2a). An embedded region between concrete and steel and concrete and GFRP bars was considered.

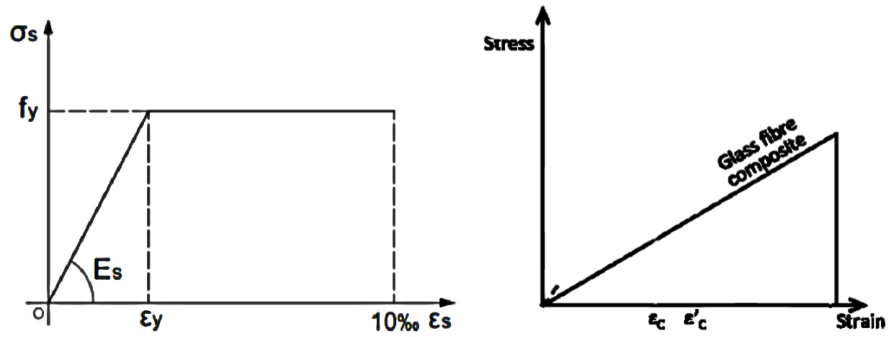

Figure 2. Stress-strain diagram of (a) Steel (Pinheiro et al., 2020), (b) GFRP (Swolfset al., 2016).

The properties of the bars adopted were the modulus of elasticity (E), tensile strength (f_{fu}) and yield strength (f_{yd}), which were obtained from the studies by Dalfré et al. (2021) and are shown in Table 2. Other values such as modulus of elasticity and stress-strain relationships were obtained through formulations presented subsequently.

Table 2. Bars properties.

Material	E (GPa)	f_{fu} (MPa)	f_{yk} (MPa)	Rupture strain (%)
GFRP	48	1047	-	2.18
CA-50	210	-	500	-
CA-60	210	-	600	-

In the study conducted by Dalfré, et al. (2021) simulations were carried out on four different beams. Two of these beams were designed with the partial incorporation of GFRP, as a substitute for the lower steel reinforcements. The structural composition of the beams consisted of two 6.3 mm CA-50 steel bars as the upper longitudinal reinforcement, as well as two 10 mm GFRP bars as lower longitudinal reinforcement adopted as partial replacement. In addition, the beams were equipped with transverse reinforcement made from CA-60 with a diameter of 5 mm.

The total length of the beam modeled was 250 cm, with a rectangular cross-section 12 cm and 20 cm width and depth, respectively. The effective span adopted was 230 cm. Cover thickness adopted was 1,5 cm and the structural design was conducted following the guidelines of American Concrete Institute 440.1R (ACI, 2015). Figure 3 illustrates the dimensions of the beam used in the simulation.

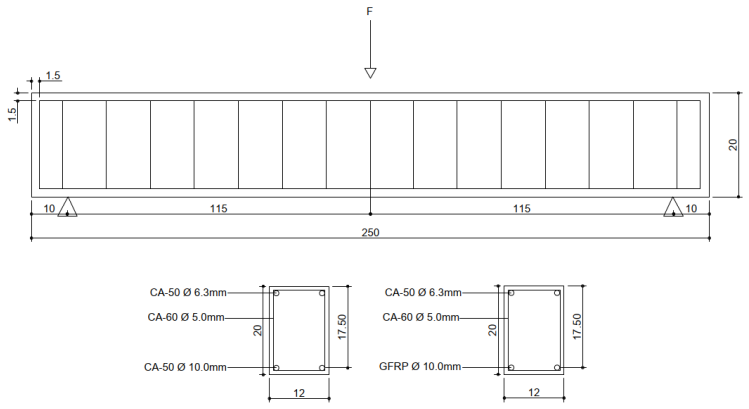

Figure 3. Detailing of the tested beams. Adapted from Dalfré et al. (2021).

For the model with GFRP bars, the concrete beam was simulated with hexahedral solid elements without reduced integration (C3D8) with a mesh size of 40 mm, while the transverse and longitudinal reinforcements were simulated as bar elements (T3D2) with 40 mm meshes. The 25, 30, 35 and 40 mm meshes were tested, and the model with the 40 mm mesh showed the closest behavior to that obtained experimentally. Plates were used as rigid analytical models, representing the supports and the point of load application. A reference point for the application of displacement was defined through the plate, as obtained in the studies by Dalfré, et al. (2021). The simulation was conducted considering the vertical displacement obtained in the experimental models, with the resultant force of this displacement being measured at the end of the simulation. This displacement was performed incrementally.

For the model with steel bars, the concrete beam was simulated with hexahedral solid elements with reduced integration (C3D8R), with 15 mm, and the longitudinal bars and stirrups were simulated as unidirectional bar elements (T3D2) with 50 and 10 mm respectively. This configuration is widely considered in similar simulations (Raza et al., 2019; Gemi et al., 2021).

For both models, the interaction of the bar elements with the concrete and the contact condition adopted was embedded region, present natively in the program (Dassault Systèmes Simulia, 2012), consisting of an incorporation of the longitudinal and transverse reinforcements into the concrete beam.

Concrete Damage Plasticity (CDP)

According to Spozito et al. (2024), the damage or failure behavior of concrete can be defined using models available in the Abaqus software, one of which is CDP. CDP is able to reproduce the inelastic behavior of concrete by combining the concept of isotropic elastic damage with isotropic traction and plastic compression.

The CDP model, in short, consists of replacing the commonly used strength variable with the plastic damage variable, which only increases if the plastic state of deformation arises. However, this increase must be limited, since once this limit is reached, the behavior obtained will be that of total damage, which will cause cracking (Lubliner et al., 1989).

In the Abaqus software, the parameters required for the CDP are the angle of dilation, the eccentricity, the ratio between the biaxial and uniaxial compressive yield stresses, the ratio of the second invariant stress in the tensile meridian and the viscosity parameter. When proposing the CDP, Lubliner et al. (1989) defined the yield criterion, the most commonly used criteria being Mohr-Coulomb and Drucker-Prager, which can be defined in Equation 4:

$$F(\sigma) = c \tag{4}$$

Where $F(\sigma)$ is the homogeneous function in the first degree of the stress components and c is the cohesion. Given the low correlation with experimental and geometric data, this equation underwent several improvements and was later modified by Lee and Fenves (1998) in Equation 5.

$$F(\sigma) = \frac{1}{1-\alpha}\left[\sqrt{3J_2} + \alpha I_1 + \beta < \sigma_{máx} > -\gamma < -\sigma_{máx} >\right] \tag{5}$$

Where:

$\sigma_{máx}$ = Maximum principal stress.

I_1 = Sum of the principal stresses in a stress state.

J_2 = Intensity of the deviatoric stress in a stress state.

Where α, β and γ are dimensionless constants, α (Equation 7) being obtained from the comparison of the yield stress at biaxial and uniaxial compression f_{bo} and f_{co} (Equation 6).

$$\frac{f_{b0}}{f_{c0}} = \frac{1-\alpha}{1-2\alpha} \tag{6}$$

$$\alpha = \frac{(f_{b0}/f_{c0})-1}{2(f_{b0}/f_{c0})-1} \tag{7}$$

Using the ratio of the uniaxial compressive yield strength and the uniaxial tensile initial yield strength (Equation 8), it is possible to obtain the value of β.

$$\frac{f_{b0}}{f_{c0}} = \frac{1+\alpha+\beta}{1-\alpha} \tag{8}$$

Rewriting the previous equation, emphasizing the variable β, gives equation 9.

$$\beta = (1-\alpha)(f_{c0}/f_{b0}) - (I+\alpha) \tag{9}$$

The CDP model also considers non-associated potential plastic flow. The potential flow G that is adopted by the model consists of the hyperbolic Drucker-Prager function, which is represented by Equation 10.

$$G = \sqrt{\in \sigma_{t0}\, tan\, \psi)^2 + \bar{q}^2} - \bar{p}\, tan\, \psi \quad (10)$$

Where:

ϵ_t = Uniaxial tensile stress at failure.

Ψ = Dilation angle.

$\bar{q}$ =Mises equivalent effective stress.

$\bar{p}$ = The hydrostatic pressure stress.

For this study, the constitutive model proposed by Guo (2014) was utilized to represent the concrete behavior under tension and compression, including damage in both regimes. The parameters adopted for the CDP were 20° for the angle of dilation, 0.1 for eccentricity, 1.16 for the ratio between biaxial and uniaxial compressive yield stresses, 0.667 for the ratio of the second invariant stress in the tensile meridian, and 0.0001 for the viscosity parameter. For validation of the model using the CDP, several tests were proposed by varying the parameters of angle of dilation and viscosity, which are among the most varied parameters in the literature (Silva et al., 2021).

Results and discussion

This chapter presents the results obtained in this study, starting with the presentation of the validation of the numerical model, followed by the results of the parametric study and ending with the analysis of the failure mode.

Numerical model validation with CDP

The experimental model by Dalfré et al. (2021) using steel and GFRP was evaluated in terms of the force-deflection curve and the cracking it showed. Regarding the displacement values obtained from the numerical model, they were measured from the lower face of the critical cross-section (center of the beam). The maximum values were considered. Figure 4 shows the behavior obtained in the numerical model using longitudinal steel bars compared to the experiments carried out in the laboratory by the authors.

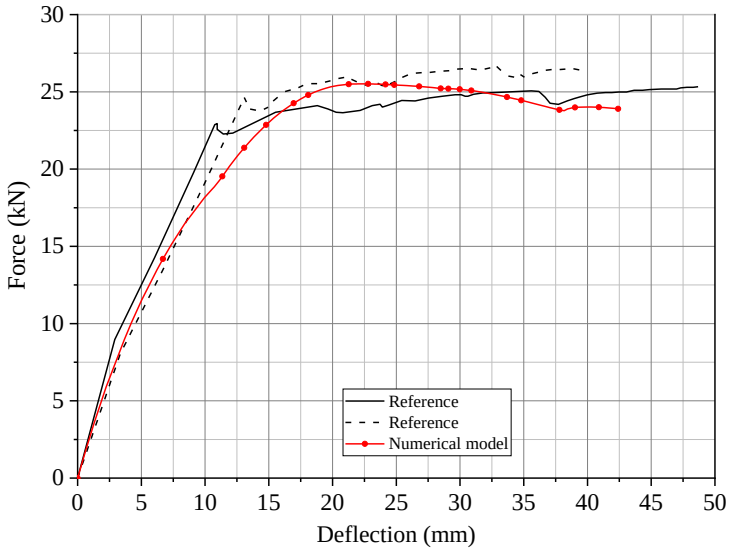

Figure 4. Load-deflection graph of mode using longitudinal steel bars.

The force-deflection curve of the numerical model shows good agreement with the experimental models analyzed, the maximum load (F_{max}) supported in the numerical simulation was 25.51 kN, while the average result of the reference was 25.97kN. Thus, an error of 1.77% can be observed between the experimental and numerical models, an adequate value when compared to international literature (Ji et al. 2021).

The same analysis was carried out for the model using GFRP, the numerical model was compared to the experimental models using GFRP bars, obtaining the force-deflection curve as shown in Figure 5.

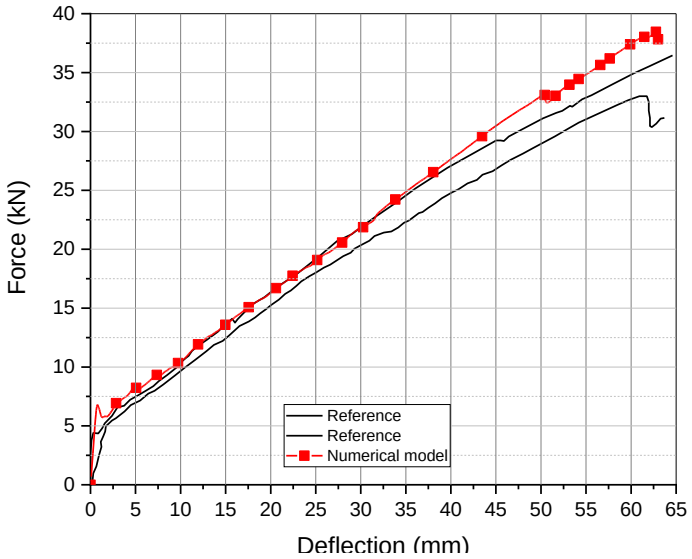

Figure 5. Load-deflection graph of GFRP model.

The numerical model also showed good agreement when compared to the experimental results. The maximum load of 37.64 kN was obtained for the numerical model, while the average maximum load of 35.22 kN was obtained for the experimental model, with an error of 6.87%. It can therefore be concluded that both models were able to represent real mechanical test situations.

CDP was used to consider the constitutive model of concrete. This model shows good agreement when used to represent the inelastic behavior of concrete (Raza et al., 2019), as well as making it possible to verify the damage in the model, both in tension and compression (Guo, 2014).

As presented by Dalfré et al. (2021), the use of GFRP bars as a partial replacement for the lower longitudinal bars resulted in an increase in bearing capacity, given the high strength of GFRP bars compared to steel. On the other hand, this substitution resulted in a crushing rupture of the concrete, since GFRP bars are fragile materials with abrupt rupture, so it is imperative to take advantage of the concrete's capacity when subjected to compression, so that the bars do not collapse. The same result was numerically obtained, showing conformity with the studies by Dalfré et al. (2021).

Parametric study results

Twenty-four simulations were carried out using the validated model, varying only the properties analyzed in this study in order to understand and analyze the behavior as the parameters varied. For the model where only steel was used, the following behavior was obtained for the force-deflection curve (Figure 6).

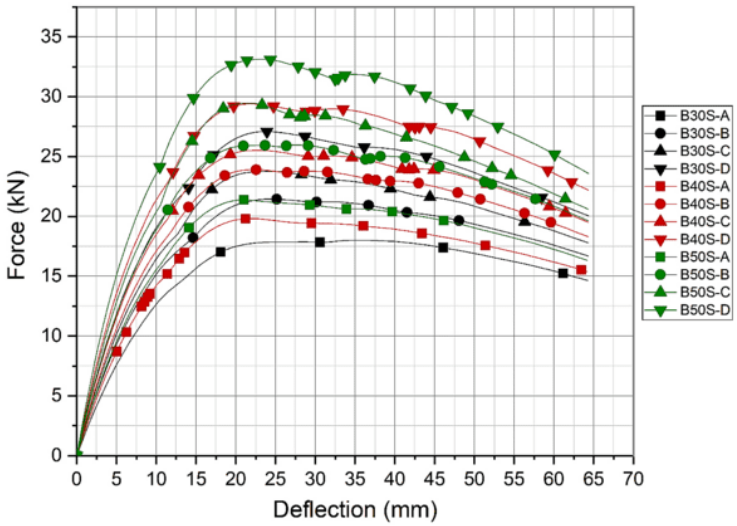

Figure 6. Load-deflection graph of parametric steel models.

It can be seen that as the modulus of elasticity rises, there is a significant increase in the element's load capacity. Evaluating the variation in maximum load between the extremes, B30S-A to B50S-D, there was an 83.93% increase in load capacity, an increase that can be explained by the increase in modulus of elasticity in conjunction with f_{ck}. Among the models, when analyzing the variation in f_{ck} while maintaining the same alpha, it is possible to observe a notable increase in loadbearing capacity, the best increase occurring among the models where f_{ck} of 30 MPa and 50 MPa were used, The best result was the comparison between models B30SC and B50S-C, where the variation in f_{ck} generated a 23.90% increase in loadbearing capacity, followed by the relationship between models B30S-D and B50S-D and B30S-B and B50S-B, which obtained an increase of 22.27 and 21.13%, respectively.

When the f_{ck} is maintained and only the alpha is varied, it is possible to see a greater percentage increase between the models. The ratio between the B30S-A and B30S-D models generated an increase in load capacity equivalent to 50.42%, while the variation in alpha and in the models where 40 MPa was adopted led to an increase of 48.37%, and finally, in the models adopting 50 MPa, the increase in load capacity was 55.06%.

It is noticeable that varying the aggregate to be used causes a considerable increase compared to the increase obtained by varying the f_{ck}, demonstrating that the use of varied aggregates can bring a better benefit to the mechanical behavior of concrete, depending on their availability in the region. This variation presents itself as an economically favorable method, since the investment in higher concrete strength classes is much higher than the investment in other types of aggregate.

When GFRP is used in the lower longitudinal reinforcement, the load capacity already shows a considerable increase (Figure 7). When comparing the average maximum loads of the models made using steel, it can be seen that the models using GFRP resulted in a 63.97% increase in the average maximum load. This result when using GFRP can be explained by the high strength of the of the fibers, which, when used in concrete elements, can increase their capacity to resist stress (Del Savio et al., 2023). Its low deformability also results in a reduced contribution of the concrete to the overall load-bearing capacity, thereby justifying a higher load capacity.

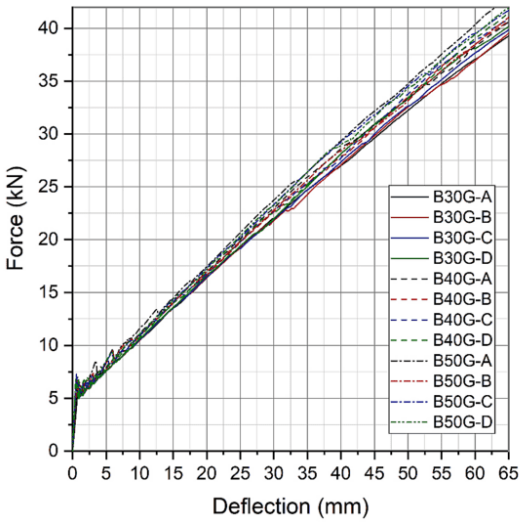

Figure 7. Load-deflection graph of parametric GFRP models.

The difference obtained at the extremes of the highest and lowest modulus of elasticity, i.e. B50G-D and B30G-A, respectively, was a 6.28% increase in the maximum load. GFRP, in contrast to steel, shows the opposite behavior when the f_{ck} is kept fixed and only the alpha e is varied, this change does not lead to significant increases, with an increase of 2.27% for the models using 30 MPa and 2.11% for the 40 MPa models. In this evaluation, the most significant increase occurs when the f_{ck} is increased, with the best result being the comparison between the B30G-A and B50G-A models, providing a 9.44% increase in maximum load capacity, followed by a 5.88% increase in the load capacity of the B40G-A model when compared to the B50G-A model. This change in behavior can be explained by the ductility of the GFRP bars. As it is a brittle material, it is necessary for the concrete to have a higher compressive strength so that the bars behave properly and do not reach brittle rupture.

The ratio between the B50G-A and B50G-D models using 50 MPa showed a 2.49% reduction in the maximum load capacity as the alpha variation was adopted. This factor can be explained by the low modulus

of elasticity of the bars, causing an increase in the concrete's compressive stresses. Figure 8 shows the variation in behavior with the change in alpha e for the beams with f_{ck} equal to 50MPa.

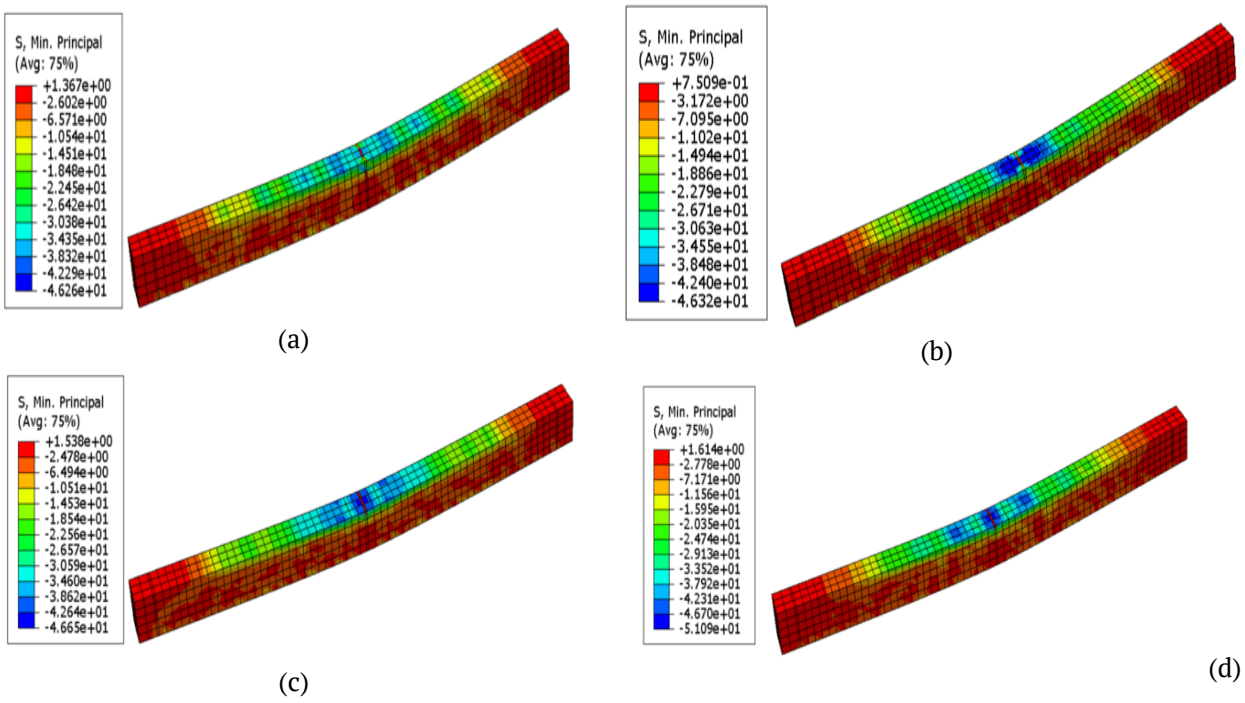

Figure 8. Compression stresses (a) B50G-A (B)B50G-B (C) B50G-C (D) B50G-D.

As can be seen in Figure 9a, the steel RC beam used as a reference for this study, under the Fmax of 25.95 kN, reached a plasticity percentage of 1.08 %, entering the yield point, which occurs at 1.0% (ABNT, 2014), beam B50S-C showed the same value for Fmax of 25.52 kN. According to the normative document ACI 440.1R (2015), the average rupture percentage for GFRP ranges from 1.2 to 3.1. For the beams using GFRP, the reference beam had a percentage of 1.59 for a maximum force of 37.64 kN, while the stiffer beam modeled for this study had a percentage of 1.76% under the maximum force of 42.98 kN, exceeding the minimum value mentioned in ACI 440.1R, but still below the average rupture value of 2.15%.

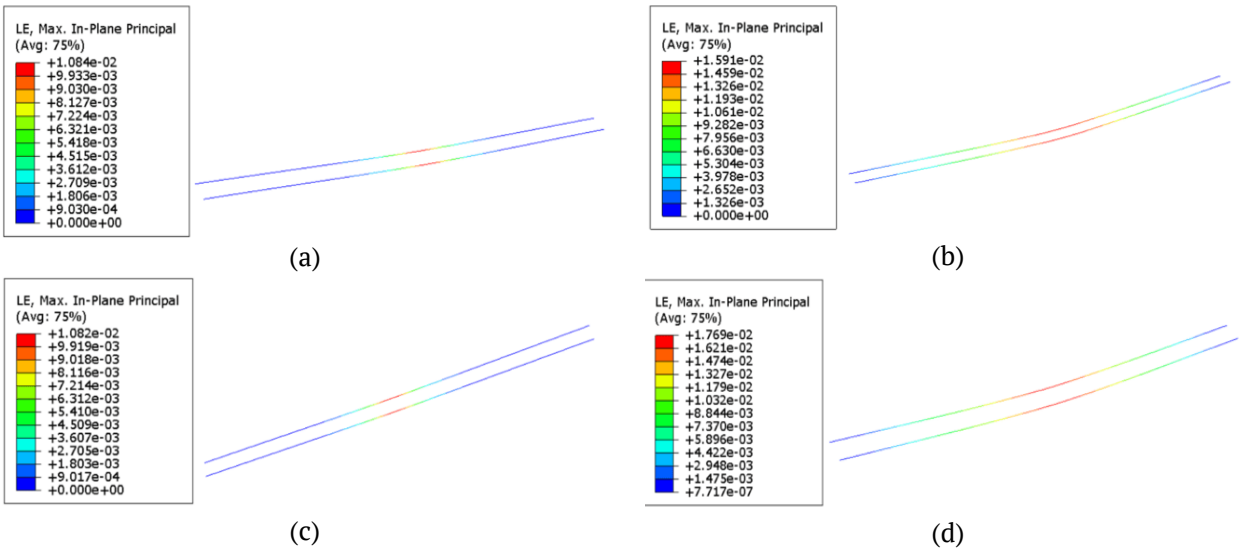

Figure 9. Plastic deformation in the lower reinforcement (a) Steel reference (b) GFRP reference (c) B50S-C (d) B50G-A.

When analyzing the plastic behavior obtained in concrete, ABNT NBR 6118 (2023) presents the percentage of maximum deformation of the fibers as 0.35%, as can be seen in the reference model that was simulated (Figure 10a), the concrete reaches the value of 0.37%, that is, it is within the state of maximum deformation,

while the model of greater rigidity using steel (B50S-C), is close to reaching the deformation point (Figure 10c), with a difference of 12.9% of the deformation point. On the other hand, the reference model, where GFRP was used, obtained a value of 0.20% (Figure 10b), while the stiffer model using GFRP obtained 0.56%, i.e. it exceeded the initial value by 60% (Figure 10d). Regarding the plastic deformation of the concrete, the positive values indicate compression.

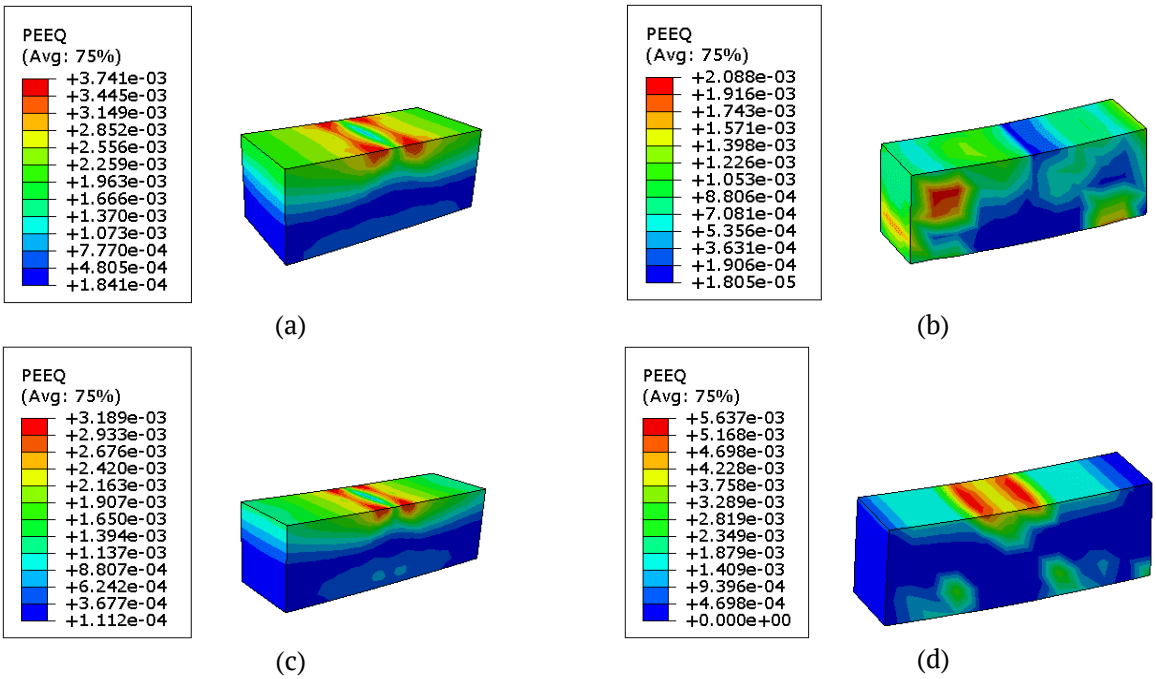

Figure 10. Plastic deformation of concrete (a) Steel reference (b) GFRP reference (c) B50S-C (d) B50G-A.

By evaluating the elastic behavior of the bars in conjunction with the behavior of the concrete in the same increment, it is possible to understand the failure mode of the element. For the reference beam using steel, the bars have reached the yield point together with the start of plastic deformation of the concrete, both are in a state of deformation, the concrete has ceased to support the stresses and now the steel is in demand. In the B50S-C model, the behavior shows failure due to reinforcement yielding, since the steel reinforcement began to yield at Fmax, while the plastic deformation of the concrete was not reached.

For the reference using GFRP, the concrete has not reached the maximum deformation, with values close to 0.105%; on the other hand, the GFRP bar is already between the rupture values, but has not yet reached the average value of 2.15%. In the B50G-A model, the concrete has already passed the point of maximum deformation, while the GFRP bars have not yet reached the average rupture value, corroborating the study by Srihari et al. (2017), that the use of GFRP bars must be carried out with the concrete's compressive strength as a critical factor, given the bars' fragile mode of rupture.

In addition to the plastic deformation, the stresses obtained in the elements when subjected to maximum load were evaluated and compared with the critical stresses. The behavior of the lower reinforcements and their respective stresses is shown in Figure 11.

When evaluating the stress obtained when the element was subjected to maximum load, it can be seen that the models where steel was used as the lower reinforcement exceeded the critical stress of 500 MPa, with both the simulated reference model and the B50S-C model reaching 545 MPa at the point of maximum load. When GFRP was used in the lower reinforcement, the stress increased to 811 MPa in the reference model and 902 MPa for the stiffer B50G-A model, but did not reach the critical stress. of the GFRP bars corresponding to 1047 MPa (Dalfré et al., 2021).

Finally, the maximum concrete compressive stresses were analyzed, as shown in Figure 12. It was possible to observe a discrepancy between the numerical models: for the steel, the maximum stress obtained in the middle of the span exceeded 100MPa, but both models had already exceeded the yield strength of the steel bar, so it can be concluded that the concrete at the point analyzed in Figure 12a and Figure 12b was already under total rupture. On the other hand, the model using GFRP is closer to the f_{ck} of the concrete. The reference model showed

25.64 kN, 21.82% less than the value adopted by the authors Dalfré et al. (2021). In the B50G-A model, the maximum stress at certain points reaches 46.26 MPa, a reduction of 7.48% on the f_{ck} value adopted.

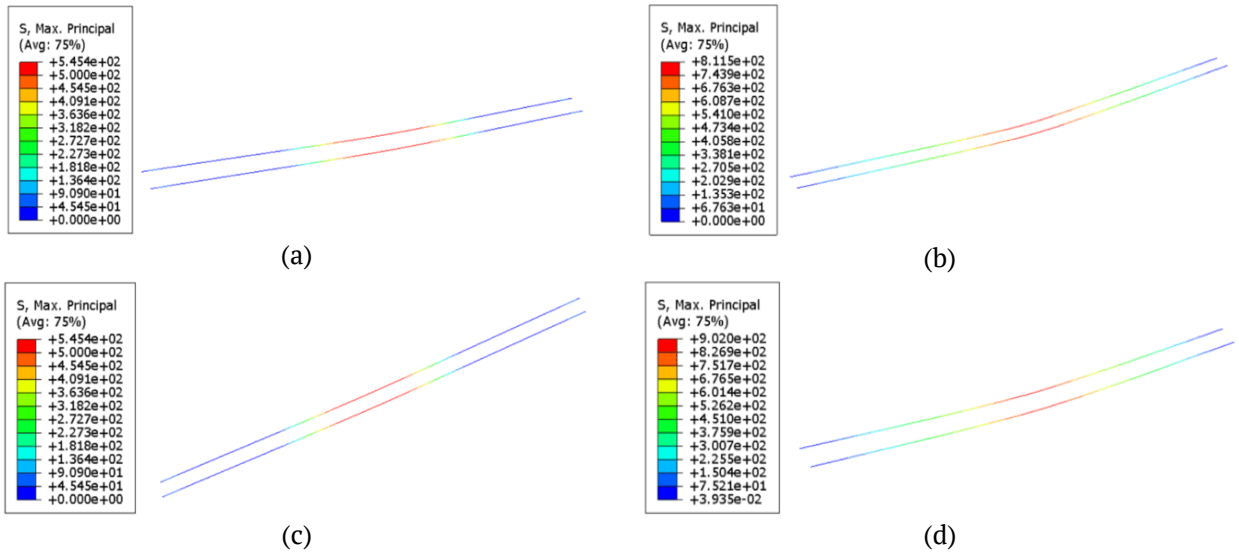

Figure 11. Maximum tensile stresses (a) Steel reference (b) GFRP reference (c) B50S-C (d) B50G-A.

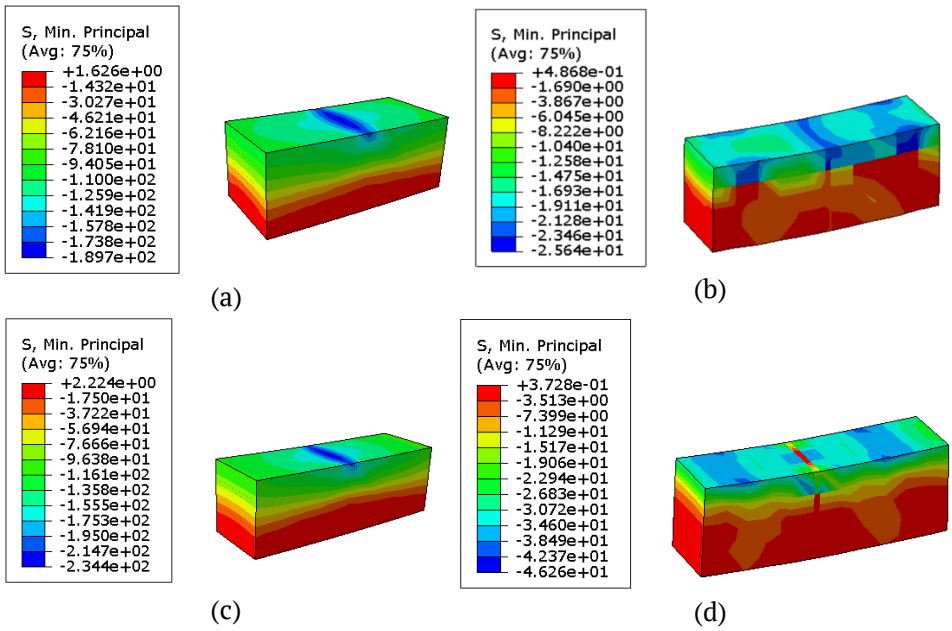

Figure 12. Maximum compressive stresses (a) Steel reference (b) GFRP reference (c) B50S-C (d) B50G-A.

Conclusion

Through this research it was possible to understand that due to the proximity between experiment and numerical simulation, the use of FEM demonstrates a good capacity for modeling structural elements, as well as the results obtained through the available software. With the help of FEM, it is possible to overcome the difficulties of experimental models which, in the case of GFRP bars, consist of obtaining the bars or manufacturing them in the laboratory.

As can be observed, the model is an approximation of the experimental result. Given the difficulties in obtaining the mechanical properties correctly and the lack of standardization, the behavior tends to vary greatly depending on the values entered into the Abaqus software database. All these factors must be observed during the validation process, since they directly influence the behavior that will be obtained in the force-deflection curve.

In the case of concrete, the use of CDP shows good compatibility in representing the behavior of concrete and also the damage that occurs during the application of displacement. The adoption of CDP shows efficiency

when adopted for concrete, as observed in the studies by Alam and Hussein (2020) and Sun et al. (2019). The analysis shows that:

- There is a change in the failure mode depending on the material used for the bottom reinforcement. In the case of steel, the common failure mode is the yielding of the reinforcement, while in GFRP the failure mode is the crushing of the concrete.
- The use of the finite element method showed good agreement with the models carried out experimentally, demonstrating that the FEM can be used to simulate structural elements if validated correctly, eliminating or mitigating the need to carry out experiments in the laboratory, which are highly complex due to the need for specific equipment and materials for their development.
- GFRP has demonstrated its ability to be used as a lower reinforcement in structural elements, making better use of the concrete's compressive strength, as well as increasing the maximum load capacity to be supported by the beam.

References

Alam, M. S., & Hussein, A. (2020). Idealized tension stiffening model for finite element analysis of glass fibre reinforced polymer (GFRP) reinforced concrete members. *Structures*, *24*, 351-356. https://doi.org/10.1016/j.istruc.2020.01.033

Alves, G. F. T., Amaral, V. G. H., Jardim, P. I. L., & Almeida, D. H. (2024). Análise numérica da influência do módulo de elasticidade do concreto na rigidez de vigas de concreto armado com barras de GFRP. *Revista de Engenharia e Tecnologia*, 16(1), 1-9.

American Concrete Institute [ACI]. (2015). ACI 440.1R: Guide for the design and construction of structural concrete reinforced with firber-reinforced polymer (FRP) bars.

Associação Brasileira De Normas Técnicas [ABNT]. (2013). NBR 15575: Edificações habitacionais — Desempenho Parte 1: Requisitos gerais.

Associação Brasileira De Normas Técnicas [ABNT]. (2014). *NBR 6118: Projeto de estruturas de concreto - procedimento*.

Associação Brasileira De Normas Técnicas [ABNT]. (2023). NBR 6118: Projeto de estruturas de concreto - procedimento.

Chattopadhyay, S., Rajkumar, R., & Umamaheswari, N. (2018). Analytical investigation on flexural behavior of concrete beams reinforced with gfrp rebars. *International Journal of Civil Engineering and Technology*, *9*(4), 1-8.

Dalfré, G. M., Mazzú, A. D. E., & Ferreira, F. G. S. (2021). Discussões sobre o dimensionamento de vigas de concreto armadas à flexão com barras de GFRP. *Concreto and Construções*, *XLVIII*, 79-86. https://doi.org/10.4322/1809-7197.2021.101.0008.

Dassault Systèmes Simulia. (2012). Abaqus 6.12 analysis user's manual: Prescribed conditions, constraints and interactions. *Abaqus 6.12*, *5*, 831.

Del Savio, A. A., Esquivel, D. L. T., Silva, F. A., & Pastor, J. A. (2023). Influence of Synthetic Fibers on the Flexural Properties of Concrete: Prediction of Toughness as a Function of Volume, Slenderness Ratio and Elastic Modulus of Fibers. *Polymers*, *15*(4), 909. https://doi.org/10.3390/polym15040909

Departamento Nacional De Infra-Estrutura De Transportes [DNIT]. Diretoria Executiva. Instituto De Pesquisas Rodoviárias. (2010). Manual de recuperação de pontes e viadutos rodoviários.

Gemi, L., Madenci, E., & Özkiliç, Y. O. (2021). Experimental, analytical and numerical investigation of pultruded GFRP composite beams infilled with hybrid FRP reinforced concrete. *Engineering Structures*, *244*. https://doi.org/10.1016/j.engstruct.2021.112790

Guo, Z. (2014). *Principles of reinforced concrete construction*. Elsevier.

Ineia, A., Pol, W. D. O., Braun, J. C. A., & Lopes Junior, L. S. (2021). Barras de fibra de vidro, uma alternativa inovadora e suas potencialidades: revisão bibliográfica. *Tecno-Lógica*, *25*(2), 243-251. https://doi.org/10.17058/tecnolog.v25i2.16214

Ji, J., Zhang, R., Yu, C., He, L., Ren, H., & Jiang, L. (2021). Flexural Behavior of Simply Supported Beams Consisting of Gradient Concrete and GFRP Bars. *Frontiers in Materials*, *8*. https://doi.org/10.3389/fmats.2021.693905

Lubliner, J., Oliver, J., Oller, S., & Oñate, E. (1989). A plastic-damage model for concrete. *International Journal of Solids and Structures*, *25*(3), 299-326. https://doi.org/10.1016/0020-7683(89)90050-4

Pinheiro, L. C. L., Real, M. & Magalhães, F. (2020). Comportamento do índice de confiabilidade de pilares de concreto armado em função do tempo de carregamento. *Revista Mundi Engenharia, Tecnologia e Gestão*, *5*(8). https://doi.org/10.21575/25254782rmetg2020vol5n81382

Raza, A., Khan, Q. U. Z., & Ahmad, A. (2019). Numerical investigation of load-carrying capacity of GFRPreinforced rectangular concrete members using CDP model in abaqus. *Advances in Civil Engineering*.

Ribeiro, D. V., Sales, A., Tutikian, B. F., Souza, C. A. C. De, Almeida, F. Do C. R., Cunha, M. P. T., Lourenço, M. Z., Cascudo, O., & Helene, P. (2018). *Corrosão e degradação em estruturas de concreto: teoria controle e técnicas de análise e intervenção*. Elsevier.

Silva, L. M., Christoforo, A. L., & Carvalho, R. C. (2021). Calibration of Concrete Damaged Plasticity Model parameters for shear walls. *Revista Matéria*, *26*(1). https://doi.org/10.1590/S1517-707620210001.1244

Spozito, R. S., Rodrigues, E. F. C., Santos, H. F. dos, Oliveira, I. A., Christoforo, A. L., Almeida Filho, F. M., & Delalibera, R. G. (2024). Numerical Modeling of Four-Pile Caps Using the Concrete Damaged Plasticity Model. *Buildings*, *14*(7), 2066. https://doi.org/10.3390/buildings14072066

Srihari, P., Premalatha, J., & Vengadeshwari, R. S. (2017). Finite element modeling and analysis of RC beams with GFRP and steel bars. *International Journal of Civil Engineering and Technology*, *8*(9), 671–679.

Sun, Y., Liu, Y., Wu, T., Liu, X., & Lu, H. (2019). Numerical analysis on flexural behavior of steel fiber-reinforced LWAC beams reinforced with GFRP bars. *Applied Sciences (Switzerland)*, *9*(23). https://doi.org/10.3390/app9235128

Swolfs, Y., Verpoest, I., & Gorbatikh, L. (2016). Tensile failure of hybrid composites: measuring, predicting and understanding. *IOP Conference Series: Materials Science and Engineering*, *139*. https://doi.org/10.1088/1757-899X/139/1/012008